IEEE Access
Multidisciplinary | Rapid Review | Open Access Journal

Received May 26, 2022, accepted June 9, 2022, date of publication June 20, 2022, date of current version June 23, 2022.

Digital Object Identifier 10.1109/ACCESS.2022.3184312

A 5G/Sub-Terahertz Heterogeneous Communication Network

POUYA TORKAMAN[1], GOVIND SHARAN YADAV[2], PO-CHUAN WANG[2], TUNG-YU LU[1], XUAN-WEI MIAO[1], FANG-SUNG HSIAO[1], KAI-MING FENG[2], (Member, IEEE), AND SHANG-HUA YANG[1], (Member, IEEE)

[1]Institute of Electronics Engineering, National Tsing Hua University, Hsinchu 300, Taiwan
[2]Institute of Photonic Technology, National Tsing Hua University, Hsinchu 300, Taiwan

Corresponding author: Shang-Hua Yang (shanghua@ee.nthu.edu.tw)

This work was supported by the Ministry of Science and Technology (MOST), Taiwan, through the Young Scholar Fellowship Program under Grant MOST 110-2636-E-007-017.

ABSTRACT In this paper, a heterogeneous communication system capable of delivering 5G/sub-terahertz signal carriers over an arbitrary long fiber and separated transmission links is presented by employing direct detection, multiplexing techniques, and advanced digital signal processing. In this experiment, the 3.5 GHz and 28.5 GHz carrier frequencies, representing 5G links, deliver 4 Gb/s 16-QAM OFDM signals to separate user ends over a 1-meter wireless link distance. Later, the sub-terahertz wireless communications of 4 to 10 Gb/s QPSK and 8-QAM signals with varying carrier frequencies of 125-,175- and 225 GHz, over wireless distances (<80 cm) are presented and evaluated. The results indicate that by increasing optical power from 12 dBm to 13 dBm, the bit error rate decreases two orders of magnitude. Eventually, with the assistance of artificial intelligence, a nonlinear equalizer (AI-NLE) prototype is introduced. The results indicate that the AI-NLE successfully decreases the number of errors in received data by one order of magnitude. The proposed heterogeneous system is compatible with radio-over-fiber technology, cost-effective, and easy to deploy, making it a promising candidate for indoor terahertz communication.

INDEX TERMS Artificial intelligence, broadband communication, direct detection, heterogeneous communication system, nonlinear equalizer, radio-over-fiber, terahertz communication.

I. INTRODUCTION

Terahertz (THz) frequency spectrum (100 GHz-10 THz), located between microwave and infrared spectrum, has attracted vast attention due to its wide range of applications, such as imaging, spectroscopy, and astronomy. In recent years, due to the explosive growth in mobile data, the THz spectrum has gained industrial and academic attention extensively in another area – wireless communication [1]–[3]. The advancement of wireless communications has fertilized many new technologies, including the internet of things, artificial intelligence, and virtual reality - creating exalted impacts on human society [4], [5]. There is an imperative demand for higher data-rate wireless communication systems to extend these powerful technologies' functionality and coverage range serving exponentially growing users. Since most frequency bands below 60 GHz are fully occupied due to the various applications, researchers have been investigating higher frequency bands to alleviate intensive communication traffic in the future [6], [7]. To this end, the THz band has sparked much interest due to its distinct characteristics. The THz communication network can address some critical concerns compared to its counterparts in millimeter-wave and visible light bands [6], [7].

Millimeter-wave wireless networks in the 28, 39, 60, and 73 GHz bands can sustain several Gbps within a few meters of coverage. However, the allotted bandwidth to transmit data in such systems is much less than 10 GHz, which will eventually be insufficient to support rising data demand by many emerging applications, such as 3D gaming and extended reality, inevitably pushing us to higher frequencies which lies into THz band [8]. Moreover, THz waves have shorter wavelengths compared to millimeter-wave, resulting in higher link directivity. Due to the superior directionality of the THz beam, an unauthorized user must be on the same narrow beam-width to catch messages. This will offer a platform for the provision of secure communication [8].

The associate editor coordinating the review of this manuscript and approving it for publication was Kostas Kolomvatsos.

Visible light communication (VLC) is an energy-efficient, low-cost, and non-eavesdropping method of data transmission based on mature LED technology [9]. Despite promising features of VLC, it suffers from induced noise from ambient light sources, which can drastically decrease the system performance [6]. Additionally, both receiver and transmitter should be in the line of sight (LOS). In contrast to VLC systems, non-line-of-sight (NLOS) propagation is possible in the THz band, which can serve as a backup when LOS is unattainable [6], [10]. Upon the mentioned reasons, many regards the THz frequency spectrum as the next frontier in wireless communications [10].

In a THz wireless communication system, emitter and detector characteristics significantly impact the performance of the wireless systems. In the transmitter part, two major emitter categories exist in establishing the THz wireless communication system – electronics and photonics-based devices. Electronic-based THz emitters such as frequency multiplier chains [11] and resonant tunneling diode oscillators [12] offer high output power levels, typically in the mW range and longer link distances. However, the drawback is that the maximum carrier frequencies are mainly limited to the sub-THz region, restricting the communication data rates; also, the spectrum range tunability of electronic-based THz emitters is limited to less than one-fifth of their central frequency and, therefore, the available bandwidth for data transmission, is limited [13].

THz photomixer, is one of the most promising THz active devices for high-speed wireless communication in photonics-based devices. They are compact, cost-effective, and capable of operating at room temperature. Based on the different frequencies of the two pumping laser sources, the output frequency can be accurately tuned to choose desired beating notes with several THz frequency tuning ranges leading to higher carrier frequencies and thus higher data rate. [14]. Another key advantage is its potential to integrate with already existing fiber-optic networks making this method a promising candidate for B5G/6G communication [13].

In the receiver part, high-speed Schottky barrier diodes (SBD), owing to their high sensitivity in the order of several kV/W, are widely used for THz wireless communication [15], [16]. Resonant tunneling diode (RTD) is also used in several research works due to its low power consumption and higher sensitivity compared to SBD. Most recently, Fermi-level managed barrier diode (FMB), due to high sensitivity and broadband signal detection, has also been utilized to detect THz signals [17].

Thanks to advancements in generating and detecting THz radiation technology, several research groups have already established and reported THz communication setup. A. Morales *et al.*, reported 100 Mbps data rate over carrier frequencies 80-, 120-, 160 GHz in 25 cm link distance by utilizing PIN-Photodiode (PIN-PD) photomixer as emitter and photoconductive antenna as coherent detector [18]. K. Liu *et al.*, with the assistance of a uni-traveling-carrier photodiode (UTC-PD) emitter on the transmitter side and coherent detection by a Schottky mixer and local oscillator (LO) on the reception side, reported 100 Gbps data rate with 350 GHz carrier frequency over 2-meter link distance [15]. S. Diebold *et al.*, reported a 9 Gbps data rate (286 GHz carrier frequency) over 10 cm link distance by using two RTDs as a THz emitter and a THz detector and employing a direct detection scheme [19]. J. Webber *et al.*, by using UTC-PD emitter and RTD detector, transmitted 28 Gbps data rate over 3 cm link distance per channel when the carrier frequency is set to 335 GHz [20]. T. Nagatsuma *et al.*, demonstrate a 12.5 Gbps data rate over 40 cm link distance when the carrier frequency is 300 GHz. In the proof-of-concept experiment, the authors used two UTC-PDs and FMB as emitter, LO, and detector, respectively, to do coherent detection [21]. Although the coherent detection performance is significantly better and detected power is tens of dB higher than direct detection [20], it considerably increases the complexity and cost of the system, which is undesirable in the following communication era, 6G, where the connectivity density is one order of magnitude higher than the connectivity density of 5G [2]. In recent years, besides system architecture designs, data-driven-based techniques (e.g., machine learning) combined with advanced DSP methods have also been employed to improve the performance of sub-THz and THz communication systems. W. Zhou *et al.*, designed a complex-valued neural network (CVNN) equalizer to recover 140 GHz PAM-4 signals directly from received noised data. employing a coherent detection scheme in conjugation with the proposed post equalizer significantly decreased the BER in the communication system [22]. In another research paper, to overcome the linear and nonlinear impairments of the RoF-OFDM system, C. Wang *et al.*, designed a time-frequency domain equalizer (TFDE) based on the two-dimension convolution (Conv2D) neural network (NN). The authors successfully delivered 16Gbuad 16QAM signal over 54.6 m wireless distance [23].

However, most of the state-of-the-art THz communication systems are costly, bulky, and not easy to use. To address these issues, we propose a prototype of a heterogeneous communication system that is highly compatible with the existing optical communication infra-structures to reduce additional costs while keeping the data rate sufficient for the indoor communication scheme. Here, we presented a fiber over wireless network combining a sub-THz communication system capable of covering 100 GHz spectral ranges from 125 GHz to 225 GHz with 3.5 GHz and 28.5 GHz wireless communication systems. The wavelength-division multiplexing (WDM) and THz photomixing techniques used in this heterogeneous fiber over a wireless network extensively reduce the construction and maintenance costs. Such design can simultaneously deliver numerous channels to single or different base stations, including 4G, 5G, and 6G channels. Moreover, this system can provide higher-order modulation to shrink the required bandwidth to transmit data. Using the direct detection schemes to detect higher-order modulation compared to coherent detection will also significantly decrease the cost

of the receiver side while maintaining a low required bandwidth to deliver data to users. Furthermore, by the avail of artificial intelligence, the prototype of an advanced nonlinear equalizer is introduced to minimize inter-modulation nonlinearity caused by electronics devices, significantly improving communication performance. Altogether, thanks to the employment of a compact PIN photomixer as the broadband THz emitter and an FMB diode as an ultra-sensitive and compact THz envelope detector, the proposed heterogeneous link demonstrates excellent advantages of low cost, ease of operation, ultra-broadband frequency tunability, and its scalability nature.

II. SYSYEM STRUCTURE

The proposed setup for the heterogeneous communication system is depicted in Fig. 1. The setup consists of three parts: a central office, base stations, and user ends. The transmitted signals are generated in the central office and then combined by an optical multiplexer. The combined signals will travel through an arbitrary long fiber (in our case – a 15 km single-mode fiber) and reach the small base stations. Later on, the heterogeneous signal is demultiplexed and converted to wireless signals at allocated frequency bands by RF/sub-THz emitters. The small base stations provide wireless communications to multiple mobile user devices. In the last part, we have the user end section in which detectors will detect the received signals, and then an offline process will be assisted to decode the data. To demonstrate this idea, a proof–of–concept experiment is conducted to assess the heterogeneous communication system performance and capabilities to be employed in real-life applications such as live video streaming. In this experiment, the on-off keying (OOK) format is chosen to transmit data in the sub-THz link. A higher modulation format then replaces the OOK format, and offline signal processing (DSP) is used to boost data rate while minimizing the nonlinear effects of devices and channels on the signal.

A. A 5G/mmWave/SUB-THz HETEROGENEOUS DATA LINK

In the proof-of-concept experiment, three distinct carrier frequencies transmit data signals through the wireless channel to user ends. A 3.5 GHz (mid-band) and a 28.5 GHz (millimeter-wave band) carrier frequencies, carrying 1 GHz 16-QAM OFDM data, are chosen to represent the 5G links. 3.3 to 4.2 GHz and 26.5 to 29.5 GHz frequency bands, i.e., n77 and n257, are being the most used frequency bands for 5G communication across the world compared to the other frequency bands, i.e., n258, n260, and n261. Table 1 lists several frequency bands for 5G communication technologies, along with their parameters [24].

The 125 GHz, 175 GHz, and 225 GHz carrier frequencies covering the 100 GHz spectral range demonstrate the tunable sub-THz link. To test the functionality of the sub-THz link, a 6 Gbps OOK signal is generated and successfully delivered via different carrier frequencies to the sub-THz user end. This data rate is enough to stream an uncompressed ultra-high-definition (UHD) video [25].

TABLE 1. 5G frequency bands and channel bandwidths.

Band	Common name	Uplink / Downlink (GHz)	Bandwidth (MHz)
n77	C-band	3.3-4.2	Up to 100
n257	LMDS	26.50 – 29.50	50, 100, 200, 400
n258	K-band	24.25 – 27.50	50, 100, 200, 400
n260	Ka-band	37.00 – 40.00	50, 100, 200, 400
n261	Ka-band	27.50 – 28.35	50, 100, 200, 400
n262	V-band	47.20 – 48.20	50, 100, 200, 400

The following section discusses the details of the proof-of-concept experiment. Here, inside the central office, three tunable distributed feedback (DFB) laser diodes operating in the C-band deliver optical signal carriers at 1549.964 nm, 1551.013 nm, and 1552.011 nm for the sub-THz, 28.5 GHz, and 3.5 GHz links, respectively. All output beams are delivered to a polarization controller and then into Mach-Zehnder modulator (MZM). In order to be used in the 28.5 GHz and 3.5 GHz links, two signals with 1GHz physical bandwidth and 16QAM-OFDM format are generated from arbitrary waveform generators (AWG, Tektronix 7122) and loaded into the MZM.

A pulse pattern generator (MP1763C, ANRITSU) generates a 2^{23}-1 non-return to zero pseudo random binary sequence (PRBS) signal, in the THz link. The generated PRBS signal with a peak-to-peak amplitude of 0.5 V_{pp} is connected to a modulator driver to boost the voltage to $6V_{pp}$ and load it to the MZM (bandwidth: 25 GHz). Relative to the I/Q modulator, the intensity modulator such as MZM is cost-effective with low device complexity. In an IQ modulator, two nested Mach-Zehnder modulators with a half-wave phase shifter ($\pi/2$) are combined, significantly increasing the system's price compared to MZM for indoor or device-to-device communications. Moreover, at least three bias signals are required to control the IQ modulator. Any drift in bias conditions dramatically impacts the communication performance [26]. Maintaining bias conditions in long-term usage increases the complexity of the system. Therefore, we employ a single drive MZM in our experimental setup to decrease the complexity and price of the proposed system. The insertion loss of the MZM is 4.9 dB, and the bias voltage is set at 0.97 V. Then, three signals are combined with a multiplexer and sent into a 15 km optical fiber. The optical carrier frequencies after multiplexer are monitored with an optical spectrum analyzer (AP 2060A, APEX), as depicted in Fig. 1. In the 3.5 GHz link base station, an optical attenuator is allocated to control the received optical power by a photodetector. The high-speed photodiode (PD) (PP-10G, Nortel) is assigned to convert optical signals to electrical signals. The subsequent RF amplifier is utilized to amplify the input voltage of the horn antenna (HA-08M18G-NF, FT-RF) with 16dBi gain to generate a modulated wireless signal with a central

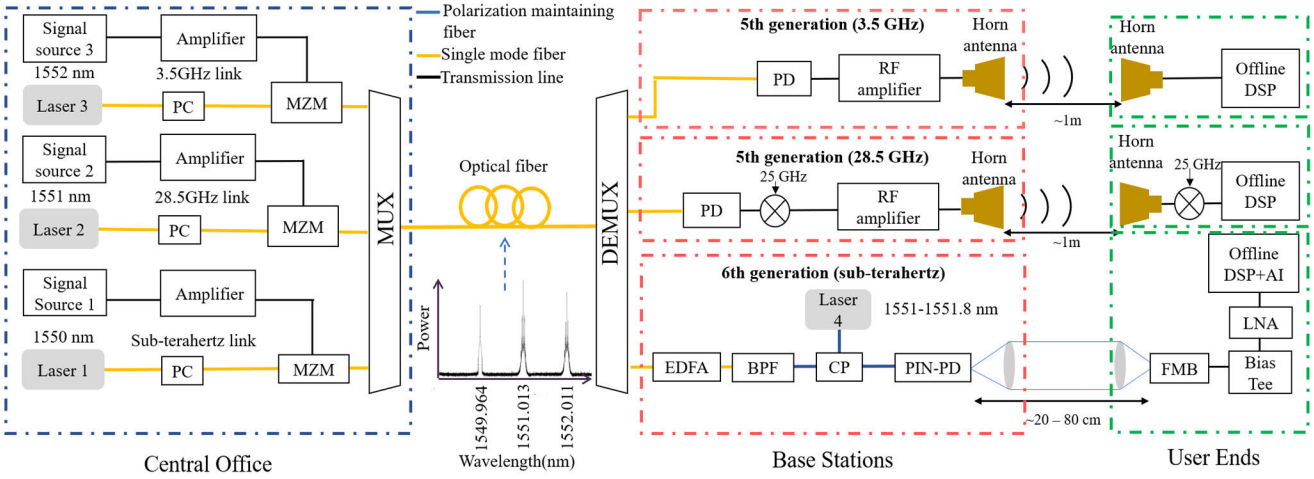

FIGURE 1. **Heterogeneous communication system. PC: Polarization controller. MZM: Mach-Zehnder modulator. MUX: Optical Multiplexer. DEMUX: Demultiplexer. PD: Photodiode. EDFA: Erbium-doped fiber amplifier. BPF: Band pass filter. CP: Optical coupler. PIN-PD: PIN-Photodiode. FMB: Fermi-level managed barrier diode. LNA: Low noise amplifier.**

frequency of 3.5 GHz. In the 28.5 GHz link base station, the electrical signal after PD is up-converted with a local oscillator by an RF mixer. Then this mmWave signal is boosted by an RF amplifier (SBL-1834034038, SAGE Millimeter, Inc.) and delivered to the horn antenna (SAR-2309-28-S2, SAGE Millimeter, Inc.) with 23dBi gain. An EDFA in the THz link base station compensates for fiber attenuation and boosts the optical power. The following band-pass filter is utilized to reject out-of-band amplified spontaneous emissions. Another C-band laser (Laser 4) serving as a local oscillator is employed for beating through the coupler. The combined optical power is delivered to the photoconductive regime of an InGaAs p-i-n photodiode (PIN-PD) (PCA-FD-1550-100-TX-1, TOPTICA PHOTONICS) to radiate a THz wave with the carrier frequency of the frequency difference between Laser 1 and Laser 4. It is worth mentioning that prior to heterodyning, a polarization controller is used to maximize the polarization-dependent conversion of PIN-PD. Currently, UTC-PD and PIN-PD are commercially available to generate THz radiation with more than -30 dBm power over a broad frequency tuning range in the sub-THz regime. As the PIN-PD presents a higher THz power level in the sub-THz regime [27], has less device complexity, and is cost-effective over UTC-PD, it could be a great candidate for large-scale sub-THz communication systems. Therefore, we utilized PIN-PD in our experiment to decrease the cost and boost the signal-to-noise ratio (SNR) in the sub-THz datalink.

In the free space transmission link, a pair of THz lenses is allocated to collimate the THz beam and reduce the propagation loss of THz signals. In the 3.5 GHz and 28.5 GHz link user ends, horn antennas receive the signals and deliver them to a real-time digital oscilloscope (28.5 GHz user end after down conversion). An offline digital signal processing is employed to demodulate the signal and calculate the bit error rate (BER) in the received data. Inside the THz link user end section, an FMB diode (IOD-FMB-19001, NTT) as an envelope detector is employed to receive the THz signal. FMB diode demonstrates very low noise equivalent power (NEP) (10^{-14} W/Hz at 300 GHz), and offers better sensitivity rather than conventional SBD receiver [21]. Later, a bias-tee filters the DC field presented in the baseband signal and the AC output signal is amplified by a 27-dB gain low noise amplifier (LNA) (BZP140B, B&Z TECHNOLOGIES) (noise figure: 4.5 dB, bandwidth: 40 GHz) for further process.

Fig. 2 presents eye diagrams of the 6 Gbps OOK signal in a different part of the heterogeneous communication system. Fig. 2(a) depicts the eye diagram of the electrical signal detected between the PRBS generator (signal source 1 in Fig. 1) and the RF amplifier. Fig. 2(b) presents the eye diagram of the optical signal after EDFA. The extinction ratio is 12.24 dB, and the RMS jitter is about 3.2 ps. Observed jitters are caused by imperfections in the behavior of the optical and electrical devices and transmission medium. Fig. 2(c) illustrates the eye diagram after the coupler, where the signal and the optical LO are combined. The extinction ratio and jitter RMS are 4.77 dB and 3.7 ps, respectively. The extinction ratio is lower compared to Fig. 2(b), where the optical LO is absent. Following the coupler, half of the optical power comes from LO and half from the optical signal, decreasing the extinction ratio. In order to investigate the frequency tunability of THz emitter, three distinct THz carrier frequencies are chosen. The eye diagrams for the test signal when the carrier frequency is set to 125 GHz, 175 GHz, and 225 GHz with a 60 cm free space link distance are depicted in Fig. 2(d ∼ f), respectively. The radiated power of the emitter diminishes as the carrier frequency increases from 125 GHz to 225 GHz. Thus, the eye begins to close. It is notable that the THz radiated power from the photomixer is quadratically proportional to the irradiated optical power. In the proof-of-concept experiment, the optical power is set to 12 dBm. In order to reach higher carrier

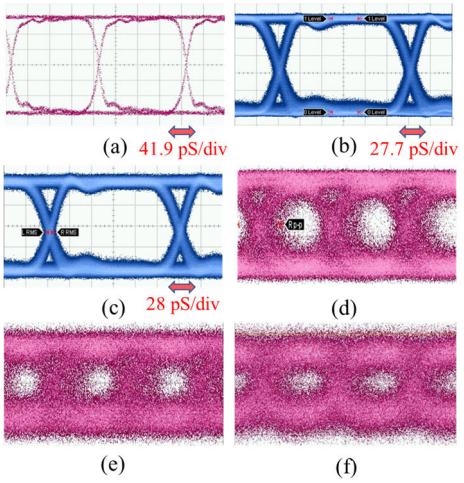

FIGURE 2. Signal eye diagrams (a) after PRBS. (b) after EDFA (c) after optical coupler. (d) after FMB when the carrier frequency is set to 125 GHz. (e) when the carrier frequency is set to 175 GHz. (f) when the carrier frequency is set to 225 GHz.

frequencies, one can push the illuminated power on PIN- PD to the nominal optical power of 15 dBm [27]. The proof-of-concept experiment demonstrates that the THz link supports different carrier frequencies from 125 GHz to 225 GHz, covering a 100 GHz spectral range. Higher-order modulations and advanced DSP codes are employed to transmit higher data rates in the following sections.

B. SYSTEM PROTOTYPE

In the proof-of-concept experiment, the signal source 1 in Fig. 1 is a PRBS generator generating a 6 GHz OOK signal; however, in the system prototype, the signal source 1 is an arbitrary waveform generator (AWG) that generates quadrature phase-shift keying (QPSK) and 8QAM-OFDM signals in order to transmit higher data rate in the sub-THz link. The detail is as follows:

In the central office, orthogonal frequency division multiplexing (OFDM) is employed to encode digital data on multiple carrier frequencies. Each sub-carrier is modulated with QAM modulation scheme and carries a part of the data. The QAM-OFDM signal is offline generated by MATLAB code, digital-to-analog converted by an AWG, and then loaded into the single drive MZM. The OFDM baseband signal can be represented as a random process with a Gaussian distribution [28].

$$s(t) = \sum_{n=0}^{n-N-1} d_n e^{(j\Delta_{\Delta\Delta nt})}, \quad \frac{2\pi}{T} = \Delta\omega, \ 0 \le t \le T \tag{1}$$

where the N is the number of sub-carriers in OFDM signal, T is OFDM symbol time, $\Delta\omega$ is angular bandwidth of sub-channel, and d_n represents the modulation format and can be expressed as:

$$d_n = A_n e^{j\varphi_n n} \tag{2}$$

The A_n and φ_n are amplitude and phase of QAM symbol, respectively. For QPSK signal $A_n = 1$ and $\varphi_n \in \{\frac{\pi}{4}, \frac{3\pi}{4}, \frac{5\pi}{4}, \frac{7\pi}{4}\}$. To generate the IQ signal and upconvert the baseband signal to intermediate frequency (IF) signal, we divide the s(t) to real and imaginary parts. Then the real and imaginary parts of signal are multiplied to $cos(\omega_{if} t)$ and $\sin(\omega_{if} t)$, respectively. Where the ω_{if} is the angular intermediate frequency. Equation (3) demonstrates the generated OFDM signal in the MATLAB.

$$\begin{aligned} s_{OFDM}(t) &= \mathrm{Re}\{s(t)\} \cdot cos\left(\omega_{if} t\right) - \mathrm{Im}\{s(t)\} \cdot \sin\left(\omega_{if} t\right) \\ s_{OFDM}(t) &= \sum_{n=0}^{n=N-1} A_n \cdot cos\left(\theta_n(t) + \omega_{ff} t\right), \\ \theta_n(t) &= \Delta\omega nt + \varphi_n \end{aligned} \tag{3}$$

where the $S_{OFDM}(t)$ is driving voltage of OFDM signal, loaded to MZM modulator. The transfer function of an ideal single drive MZN can be defined as [29]:

$$T\left(s_{OFDM}(t)\right) = \frac{E_{out}}{E_o} = \frac{1}{2} \cdot \left(1 + e^{j\left(\frac{S_{OFDM}(t)}{V_x}\pi\right)}\right) \tag{4}$$

where $E_0 = A_o e^{j\omega_o t}$ and E_{out} are input and output optical electric field, respectively; V_π is the half wave voltage of MZM; A_o and ω_o are amplitude and angular frequency of optical carrier signal, respectively. Expanding (4) into a Taylor series and keeping the linear terms, we get the output optical signal. The higher order terms in Taylor series are related to nonlinear distortion inducing intermodulation products between the subcarriers in OFDM signal band. Equation (5) shows the optical signal after MZM:

$$\begin{aligned} E_{oit} &= A_o e^{j\omega_o t} + A_T \sum_{n=0}^{n-N-1} A_n \cdot e^{j\omega_o t} \cdot e^{j\left(\theta_n(t) + \omega_{if} t - \frac{\pi}{2}\right)} \\ &\quad + A_T \sum_{n=0}^{n-N-1} A_n \cdot e^{j\omega_o t} \cdot e^{-j\left(\theta_n(t) + \omega_{if} t - \frac{\pi}{2}\right)}, \\ A_T &= \frac{A_o}{4} \cdot \frac{\pi}{V_\pi} \end{aligned} \tag{5}$$

The output signal consists of the optical carrier signal (first term) and a double side data signal (second and third terms). The output signal passes through optical fiber and reaches EDFA. After EDFA and BPF, the output signal will be heterodyned with LO laser and delivered to PIN-PD photomixer. For simplicity, we consider that the amplitude of LO is identical to the carrier optical signal, and the phase mismatch between these two optical waves is zero. However, in reality, the phase mismatch between the two free-running lasers is a source of phase noise in the received OFDM signal by the detector. The frequency of LO is slightly different from frequency of carrier signal by the desired THz frequency. The electric field of LO can be represented by (6):

$$E_{LO} = A_o e^{j(\omega_o + \omega_{THz})t}, \quad E_{copuler} = E_{LO} + E_O \tag{6}$$

And the radiated THz field from THz emitter can be modeled as (7) [30]:

$$E_{THz}(t) = R_{PN-PD}(\omega) \cdot \left(E_{coupler} \cdot E^{*}_{coupler}\right) \tag{7}$$

where the $R_{PIN\text{-}PD}$ is the responsivity of PIN-PD. It includes all the parameters related to emitter including the imbalance power between local oscillator laser and signal laser, polarization dependency, quantum efficiency of THz emitter, and the parameters of bow-tie antenna coupled to PIN-PD. After withdrawing the DC photocurrent terms and the terms with lower and higher frequencies than bandwidth of PIN-PD, the radiated term can be described as (8):

$$\begin{aligned} E_{THz}(t) = R_{PN-PD} \cdot [&2A_o^2 cos\left(\omega_{THz} t\right) \\ &+ 2A_T A_o cos\left(\omega_{THz} t\right) \sum_{n=0}^{n-N-1} A_n e^{j(\theta_n(t)+\omega_{if} t-\frac{\pi}{2})} \\ &+ 2A_T A_o cos\left(\omega_{THz} t\right) \sum_{n=0}^{n-N-1} A_n e^{-j(\theta_n(t)+\omega_{if} t-\frac{\pi}{2})}] \end{aligned} \tag{8}$$

Subsequently, the wireless THz signals are radiated and directly detected by the FMB, which is a square-law-based component. Considering the output RF bandwidth limitation of the FMB detector, the output signal can be expressed as (9) [30]:

$$\begin{aligned} E_{FMB}(t) &= R_{FMB} \cdot \left(E_{THz} \cdot E^{*}_{THz}\right) \\ E_{FMB}(t) &= R_{FMB} \cdot R^2_{TH_A}[2A_o^4 + 8A_T A_o^3 \sum_{n=0}^{n-N-1} A_n \\ &\times cos\left(\theta_n(t) + \omega_{ff} t - \frac{\pi}{2}\right) \\ &+ 4A_T^2 A_o^2 \sum_{n=0}^{n=N-1} \sum_{m=0}^{m=N-1} A_m A_n e^{j(\theta_e(t)-\theta_m(t))} \\ &+ 4A_r^2 A_o^2 \sum_{n=0}^{n=N-1} \sum_{m=0}^{m=N-1} A_m A_n \\ &\times cos\left(\theta_n(t) + \theta_m(t) + 2\omega_{if} t - \pi\right) \end{aligned} \tag{9}$$

The R_{FMB} is the responsivity of FMB. The system's channel response and impairments are not considered here to simplify the derivations. As indicated in (9), the detected signals contain a DC term (first-term), the desired OFDM signal (second-term) and the subcarrier-to-subcarrier beating interference (SSBI) component (third and fourth-terms).

The received signal after passing through LNA is given to a real-time digital oscilloscope (DSO- X 92504A, KEYSIGHT TECHNOLOGIES), and subsequently, DSP code, including down-conversion, channel estimation, equalization, phase noise compensation, and digital demodulation, is utilized to demodulate the signal offline. The key parameters of encoder and decoder are given in the Table 2.

As an example, Figs. 3(a) and (b) present the generated signal by MATLAB in the time domain and frequency domain,

TABLE 2. Encoder and decoder key parameters.

Description parameters	Values
Signal bandwidth (BW)	2-5 GHz
intermediate frequency	1.5× BW
Modulation format	QPSK- 8QAM
Cyclic prefix ratio	1/8
sampling rate of DAC	50 GHz
sampling rate of ADC	80 GHz
FFT size	1024
Number of subcarriers	[Signal BW×(FFT size × (1- Cyclic prefix ratio))]/ DAC
Pass band frequency of Low pass filter	Signal BW× 0.7
Stop band frequency of Low pass filter	Signal BW× 0.9

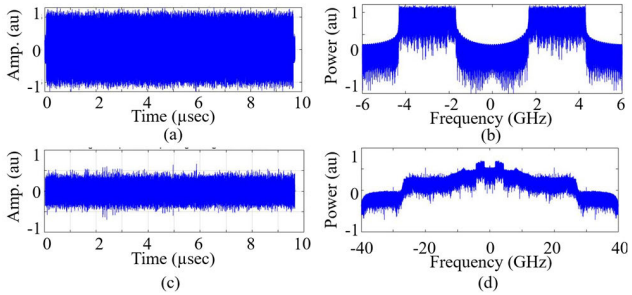

FIGURE 3. Depicts the 2GHz 8QAM-OFDM (a) generated signal in time domain (b) frequency domain. (c) received signal in time domain (d) and frequency domain.

respectively. The intermediate frequency (IF) is 3 GHz, and the signal bandwidth is 2 GHz modulated in 8QAM-OFDM. Figs. 3(c) and (d) show the received signal passing through fibers and wireless channels. The effect of channels on signal is observable in Fig. 3(d). The channel has changed the shape of the signal and partially degraded it. To compensate for such degrading effects of channel on signal and other nonlinear distortion such as intermodulation nonlinearity induced by electronic devices, we developed and introduced a prototype of an advanced equalizer. Many nonlinear equalizers based on DSP, such as least mean square or recursive least square algorithms, do not perform well in compensating nonlinear fiber impairments due to their linear decision bounds [31]. Recently, it was proposed that an AI-based mitigation model would be a viable method for mitigating these distortions in 6G communications networks [32]. Here an artificial intelligence-based nonlinear equalizer (AI-NLE) is utilized to minimize the linear and nonlinear effects of electrical and optical components on data.

III. EXPERIMENTAL RESULTS AND DISCUSSION

We used MATLAB to generate the QPSK and 8-QAM-OFDM codes in the first stage and then loaded into an AWG. Inside the MATLAB code the bit error rate is calculated by

determining the error vector magnitude (EVM). The only exception is the last part of the experiment, where the AI-NLE is applied to enhance the THz link performance. Thus, the counted BER is utilized since the estimated BER from EVM generated after machine learning algorithms is unreliable. In other words, the BER calculated by EVM is valid as long as no extra data processing is undertaken.

Due to experimental constraints, the bit number in each sequence is approximately 96000 bits. As a result, counted BER cannot accurately represent our system's performance, and the minimum BER cannot fall below 10^{-5}. It is preferred to use BER calculated from EVM to manifest the system performance. Equation (10) illustrates the relationship between the BER value of the OFDM signal and EVM, which can be used to estimate the system's performance [33].

$$BER = \frac{2\left(1-\left(\frac{1}{L}\right)\right)}{\log_2^L} erfc[\sqrt{\frac{(3\log_2^L)}{L^2-1}\cdot\frac{2}{[(EVM)^2\cdot\log_2^{2^m}}}] \tag{10}$$

where the m is modulation level which for QPSK m is equal to 2, for 8QAM m is equal to 3. L is the number of levels in each dimension of array modulation system, where for QPSK and 8QAM $L = m$.

By tuning the illuminated optical power to 12 dBm, the BER is measured for different carrier frequencies. Fig. 4 depicts the BER performance for QPSK and 8-QAM signals as a function of data rate and wireless link distance for (a) 125 GHz, (b) 175 GHz, and (c) 225 GHz carrier frequencies. By looking at the subfigures, it is observable that increasing the link distance raises the BER in all frequencies. THz beam divergence, which reduces the signal-to-noise ratio at the detector side, is the primary cause of BER degradation as the link distance increases.

Fig. 4 demonstrates that the system performance is degraded by going from QPSK (2 bits per symbol) to 8QAM (3 bits per symbol). While 8QAM modulation is more spectrally efficient than QPSK modulation, it requires a higher SNR to achieve the same BER performance because its constellation clusters are closer, and errors occur with a higher probability. Therefore, for a communication channel with no bandwidth constraints, the overall transmission performance for QPSK is better than that for 8QAM.

Fig. 4(b) illustrates the relationship between BER and link distance when the carrier frequency is 175 GHz. The radiated THz power from the emitter reduces significantly in this frequency compared to 125 GHz, and consequently, the system's performance degrades [34]. In general, the performance of a THz wireless link is primarily determined by its link power budget, which can be described using the Friis transmission formula [35]. The Friis formula, shown as (11), explains the power received by the detector that depends on link distance, carrier frequency, and the gains at the receiver and emitter sides.

$$P_R = \frac{P_T G_T G_R C^2}{(4\pi R f)^2} \tag{11}$$

where $P_R, P_T, G_T, G_R, C, f, R$, represent total power received by the detector, total power delivered to the antenna, gains at the transmitter and receiver sides, light speed in free space, the operating frequency, and the wireless distance between transmitter and receiver sides, respectively.

Form (11), it is observable that the received power by the emitter depends quadratically on the operating frequency and link distance, explaining why the performance degrades as the link distance and carrier frequency increase. Fig. 4(c) presents the BER as a function of link distances when the carrier frequency is 225 GHz. At 225 GHz, the radiated power from the emitter is decreased almost five times compared to 125 GHz, significantly reducing the system performance. As a result, the BER increases remarkably compared to previous carrier frequencies, and coherent detection is necessary to achieve better BER with the same setup. This behavior is also predictable by looking at (11).

The previous experiments were conducted under 12 dBm optical powers. Here, to show the performance of our system for different carrier frequencies under different optical power, two carrier frequencies with a 25 GHz frequency distance are chosen. These two carrier frequencies can represent two different channels in a MIMO scenario. Figs. 5(a) and (b) show BER changes regarding the optical power for 140 GHz and 165 GHz carrier frequencies, respectively. In this experiment, the link distance is fixed to 60 cm, and QPSK modulation format with 4 Gbps and 10 Gbps data rates are chosen. From this figure, it is observable that by increasing power to 13 dBm, the BER decreases by two orders of magnitudes, and with a power lower than 11.5 dBm with the current setup, the data cannot be detected. The radiated THz power from PIN-PD follows the optical pump power by second order.

This experiment indicates that to extend to a higher data rate or longer link distance, one can increase the radiated optical power on PIN-PD to obtain a higher SNR. The radiated THz power from the emitter then increases quadratically with increasing optical pump power ($P_{THz} \propto P_{opt}^2$). Therefore, the THz power is doubled by adding 1.5 dB to the optical power received by the emitter. The maximum tolerated optical power of the employed PIN-PD is 15 dBm. Hence, by increasing the optical power from 12 dBm in our experiment condition to 15dBm, the radiated THz power will increase by 6 dB. By having higher THz power, the link distance and data rate can be significantly increased.

The THz link and related outcomes were thoroughly discussed in earlier sections. In this section, we discuss the results of 5G links in the heterogeneous communication system. After optical carriers (1551.013 nm and 1552.011 nm) deliver the 1GHz bandwidth 16QAM-OFDM signals to the PDs, the PDs convert the incoming optical signals into electrical signals. The intermediate frequency of both signals is set to 3.5 GHz. Therefore, in the 28.5 GHz link base station, a mixer is required to upconvert the intermediate frequency to 28.5 GHz.

Fig. 5(c) presents the BER as the function of received optical power (ROP) by PD for the 3.5 GHz link. Without any

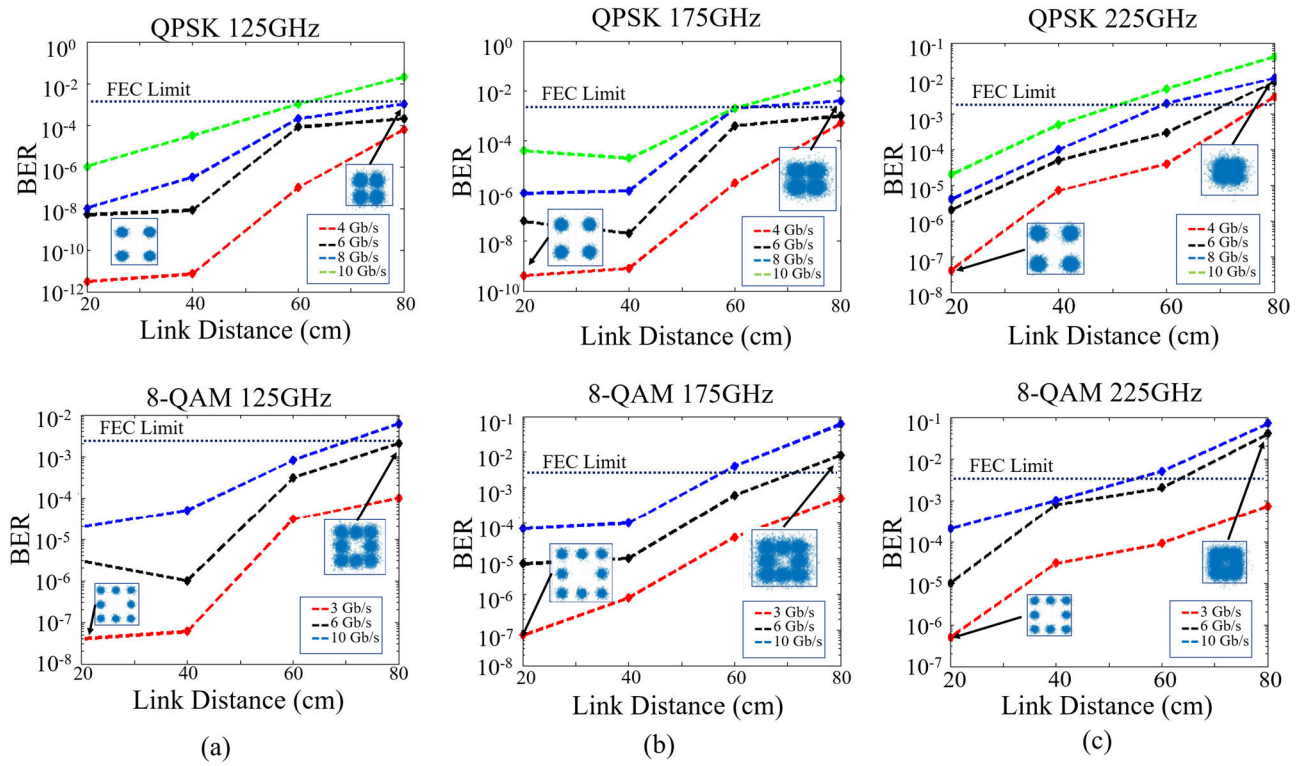

FIGURE 4. BER as a function of link distance for different data rates when the carrier frequency is set to (a) 125 GHz for QPSK and 8QAM signals (b) 175 GHz for QPSK and 8QAM signals (c) 225 GHz for QPSK and 8QAM signals. Inside the figures, the constellation diagrams for particular data rates and link distances of 20 cm and 80 cm are depicted.

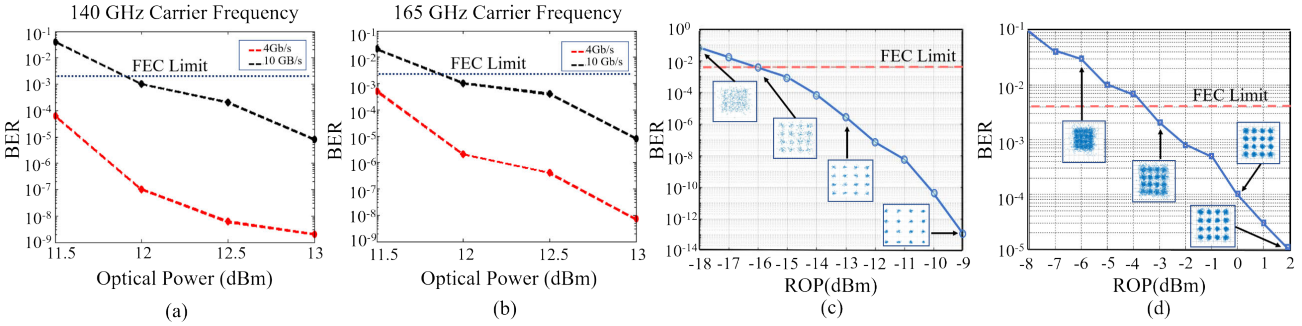

FIGURE 5. The BER versus optical power when the carrier frequency is set to (a) 140 GHz, (b) 165 GHz in the sub-THz base station. (c) BER versus ROP for the 3.5 GHz link. (d) BER versus ROP for the 28.5 GHz link. The constellation diagrams of 16QAM-OFDM transmissions for several ROPs are depicted in the inset of part c and d.

attenuation from the VOA, the maximum ROP is −9dBm, and the BER is under the hard decision forward error correction (FEC, 3.8×10^{-3} with 7% overhead) limit. The BER increases as the ROP falls until it hits the forward error correction limit of −16 dBm ROP. The presented central office can support five 3.5 GHz base stations with a power budget of 7 dB. The constellation diagrams corresponding to −9 dBm, −13 dBm, −16 dBm, −18 dBm received optical power are depicted in insets of Fig. 5(c). Fig. 5(d) shows BER versus ROP for the 28.5 GHz link. The performance, in general, is worse than the 3.5 GHz link, as to have the same BER, higher received optical power is required. This difference can be roughly explained through the Friis formula. The wireless frequency increased from 3.5 GHz to 28.5 GHz means 8.14 times higher. The received power by the detector in the Friis formula (eq. (11)) is inversely related to the frequency square. Therefore, considering all other parameters are similar between two links, the transmitted power should be increased by 64 times to have the same received power. It should be noted that Tx, Rx, amplifiers, and optical PDs for the 3.5 GHz and 28.5 GHz links are not the same; therefore, the Friss formula cannot simply be applied.

In the abovementioned experiments, traditional DSP code containing only linear equalizer is utilized to process the received signal. The linear equalizer does not perform well

to compensate for nonlinear fiber and devices impairments due to its linear decision boundaries.

IV. AI-NLE MODEL FOR SUB-THZ COMUNICATION

In recent years, the application of neural network (NN) for equalization in optical fiber transmission systems has been reported [36], [37]. However, it has not been widely used in the sub-THz communication systems. In this paper, we used an AI-NLE model as a viable solution for sub-THz communication networks. The detailed framework of training of the AI-NLE model is depicted in Fig. 6. In general, AI models have suffered from periodicity and overestimation issues. To overcome such issues, we randomly disrupt the received data set (noisy input signal and desired signal) using the random function in MATLAB to eliminate periodicity and avoid the risk of overestimation in order to completely grasp the system characteristics and signal reproducibility thoroughly [36]. To train the AI-NLE model, we randomly divided the data into three sets: training, validation, and testing, where 20% of the random OFDM symbols were used for training, 10% for validation, and the remaining random symbols for testing, as shown in Fig. 6.

As shown in Fig. 6(b), we begin by training the AI-NLE model with 20% random symbols fed into the AI-NLE model's input. To grab the AI-NLE training parameters, we train the AI-NLE model using the mean square error (MSE) criterion and acquire the training parameter using the back-propagation (BP) approach. The BP algorithm is divided into two parts. The first step is known as feedforward, in which the input signal is multiplied by the weight of each individual from the source to the destination neurons, as well as the weighting coefficient associated with each connection, w_{rn}^{l}, where l represents the l^{th} hidden layer and r, n indicate the r^{th} and the n^{th} node of the present and subsequent layer, respectively. Hence, the output signals are calculated from the input signals in this phase. It may be stated as follows [37], [38]:

$$y = x_r^l = \left(\sum_{n=1}^{M} w_m^{(l)}[\psi(\sum_{m=1}^{N} w_m^{(l-1)} x_m^{(l-2)} + b_m^{(l-1)})] + b_m^{(l)}\right) \tag{12}$$

where $x_r^{(l)}$ is the summation of all inputs to the r-th neuron at the l-th layer, $x_m^{(l-1)}$ is the summation of all inputs to the m-th neuron at the (l-1)-th layer, and w_{rm} is the noted weighting factor between two successive layers and b_1^{l-1} and b_2^l are respectively biases of AI-NLE corresponding to l and ($l-1$)-th layer. For $l = 1, x_n^{(1)}$ are the inputs of the equalizer, namely the buffered received OFDM symbols. For $l = L$, indicating the last hidden layer, $x_n^{(L)} = y_n$ are equalizer outputs. Considering system complexity, we apply only one hidden layer in the following demonstration, namely $l = 1$, 2, 3 for the input layer, the hidden layer, and the output layer, respectively. Then, to estimate the important training parameters of the AI-NLE, we employ a nonlinear activation function known as the sigmoidal nonlinear activation function, which models the system's nonlinearity. The hyperbolic sigmoid function is frequently used in data processing. In (13)-(14), the hyperbolic sigmoid function is defined as follows:

$$\psi(x) = (2 \cdot \psi_1(x) - 1) = \frac{\exp(x) - \exp(-x)}{\exp(x) + \exp(-x)} = \tanh(x) \tag{13}$$

where

$$\psi_1(x) = \frac{1}{1 + \exp(-x)} \tag{14}$$

Nonlinear activation functions are application-specific and required primarily to be differentiable. A sigmoid function is used in this AI-NLE to resolve a conflict between the boundedness and differentiability of a complex function and its hyperbolic sigmoid function values ranging from -1 to 1, as illustrated in Fig. 6(d).

The training part of BP algorithm includes both forward and backward routes to lower the mean squared error of equalizers in order to discover the appropriate weighting set $\hat{W}$ of equalizers by taking the initial guess of weights and biases of AI-NLE which is given by $W = [w_{rm}^{(l-1)}, w_{rn}^{(l)}, b_1^{l-1}, b_2^l]$ [39]. As described in (12), $\hat{W}$ is calculated using the training data, $\{y_i, d_i\}_{i=1}^{M}$ as:

$$\begin{aligned} \hat{W} &= \arg\min E(W) = \arg\min \frac{1}{p} \sum_{i=1}^{p} e_i^2 \\ e_i &= d_i - y_i \\ E(W) &= \frac{1}{p} \sum_{i=1}^{p} e_i^2 \end{aligned} \tag{15}$$

p stands for the quantity of training data, while y_i, d_i stand for the i_{th} noisy training data and desired data, respectively.

The BP method employs the steepest descent technique to minimize (15) in terms of AI-NLE weights and biases, W. The steepest descent approach requires us to calculate the partial derivative of the squired error signal $E(w)$, which is randomly initialized and then iteratively updated as [40]:

$$W(n+1) = W(n+1) - \eta \frac{\partial E(W)}{\partial W} \tag{16}$$

where η is referred to as the step-size of the learning algorithm and n is an iteration number.

The AI-weights NLE's are updated by utilizing the back-propagation algorithm (BP), which minimizes the difference

TABLE 3. AI-NLE used parameters.

Description parameters	Values
Number of input layer neurons	25
Number of hidden layers	1
Number of hidden neurons	16
Number of output layers neuron	1
Activation Function	Hyperbolic Tangent
Learning Algorithm	Adaptive Backpropagation Algorithm
Learning factor	0.001

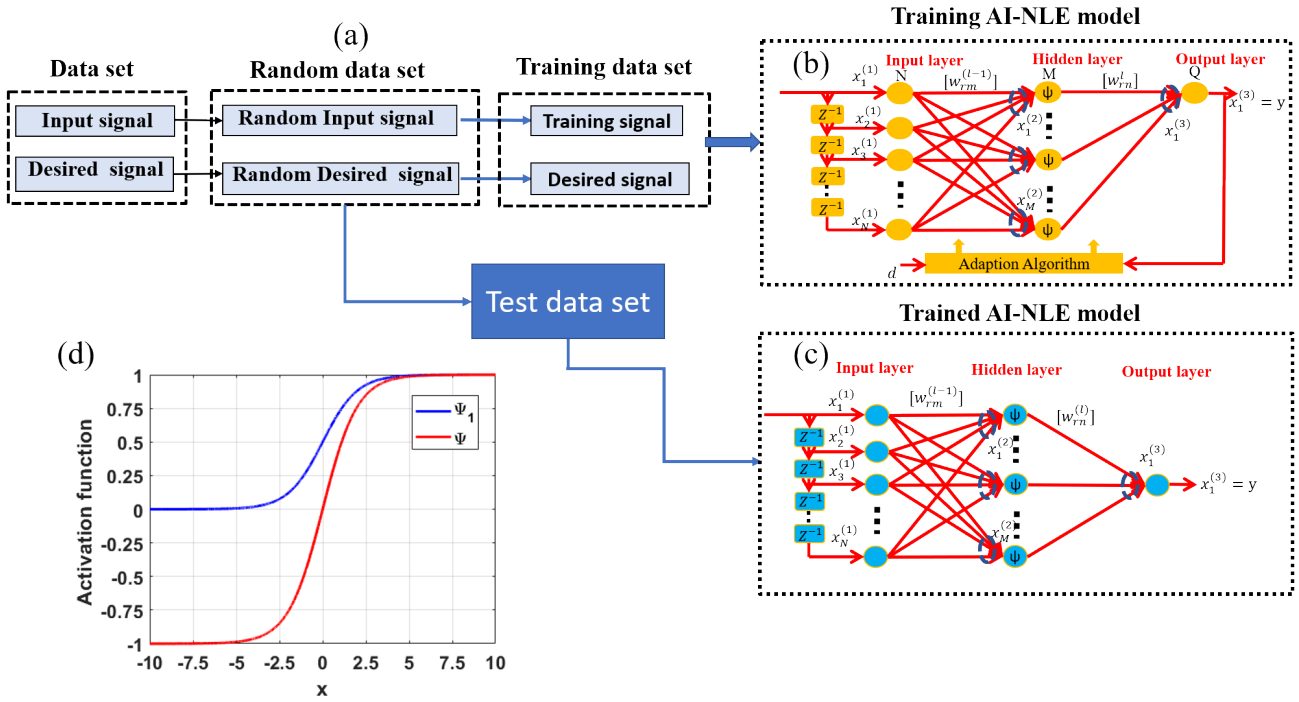

FIGURE 6. Conceptual training frame work of AI-NLE model. (a) training data set. (b) Training AI-NLE model. (c) Trained AI-NLE model (d) activation functions (sigmoidal function (blue) and hyperbolic function (red)). AI-NLE model contains N- input neurons, M-hidden neurons. Q- output neurons.

TABLE 4. Comparison of different equalization schemes.

DSP solutions	Detection scheme	Modulation format	Complexity in multiplications		Best BER performance
			General complexity	Actual complexity	
Linear equalizer (LE) [32]	Direct	16-QAM	$2N_1+1$ Where N_1 is memory length of equalizer	51 where N_1=25	7.2e^{-2}
Volterra nonlinear equalizer (VNLE) [32]	Direct	16-QAM	$N_1 + N_2(N_2+1) + \frac{1}{2}N_3(N_3+1)(N_3+2)$ N_1, N_2 and N_3 – are first, second and third order memory length	1035 where N_1=25, N_2=25, and N_3=8	1e^{-2}
Demonstrated AI-NLE	Direct	8-QAM	$N \times M + M + M \times Q + Q$ N= input neurons M= hidden neurons Q= output neurons	433 where N=25, M=16 and Q=1	1e^{-3}

between the AI-NLE output and the desired output, and then finding the ideal values using the steepest descent technique of the cost function (16). After the training has been completed. Then, in Fig. 6(c), weight coefficients are used to apply testing to merely forward propagation (FP). Table 3 presents the AI-NLE general parameters, including learning factor, learning algorithm, and the number of neurons.

The results reveal that the AI-NLE improves the BER by an order of magnitude when compared to the linear equalization technique. In table 4 our method is compared with a linear equalizer and Volterra nonlinear equalizer presented in [30]. The table shows that while the performance of AI-NLE is excellent, the complexity of the equalizer compared to the Volterra equalizer is not high.

Here, we compare the BER performance of the proposed AI-NLE prototype with linear equalizers. The BER performance as a function of link distance (cm) for a 15-km transmission at an ROP of 12 dBm is shown in the Fig. 7. The received signal suffers from many degrading effects that restrict signal quality. A linear equalization is not a viable solution for high-capacity transmission networks, as shown in Fig. 7. While, when the system's nonlinearity distorts the signal at higher data rates, our suggested AI-NLE beats the linear equalizer (LE). Both equalizers provide excellent error-free connections at lower data speeds or shorter link lengths. The proposed prototype of AI-NLE presents realistic principles for effectively regulating nonlinear aberrations in the 6G communication system.

The specifications of the proposed communication system compared to other system structures are presented in table 5. There is a trade-off between cost, simplicity, datarate, and wireless link distance. We presented heterogeneous communication systems utilizing an AI-NLE equalizer to retain the data rate sufficient for indoor and device-to-device communication while keeping the communication system

TABLE 5. THz wireless communication systems.

Type	Distance	Data rate	Carrier frequency	Emitter	Receiver	Modulation	Detection scheme	Cost	Size	Ref
Hybrid	0.5 m	100 Gb/s	300 GHz	PIN-PD	MMIC	16QAM	Coherent	High	Compact	[36]
Hybrid	1 m	5.5 Gb/s	138 GHz	PIN-PD	ZBD	OOK	Direct	Medium	Compact	[15]
Photonics	0.25 m	0.1 Gb/s	80-120-160 GHz	PIN-PD	PCA	BPSK	Coherent	High	Large	[19]
Electronics	0.1 m	9 Gb/s	286 GHz	RTD	RTD	OOK	Direct	Medium	Compact	[20]
Hybrid	0.4 m	12.5 Gb/s	300 GHz	UTC-PD	FMB	OOK	Coherent	High	Large	[22]
Hybrid	0.8 m	10 Gb/s	125-150-175 GHz	PIN-PD	FMB	QPSK-8QAM	Direct	Medium	Compact	This work

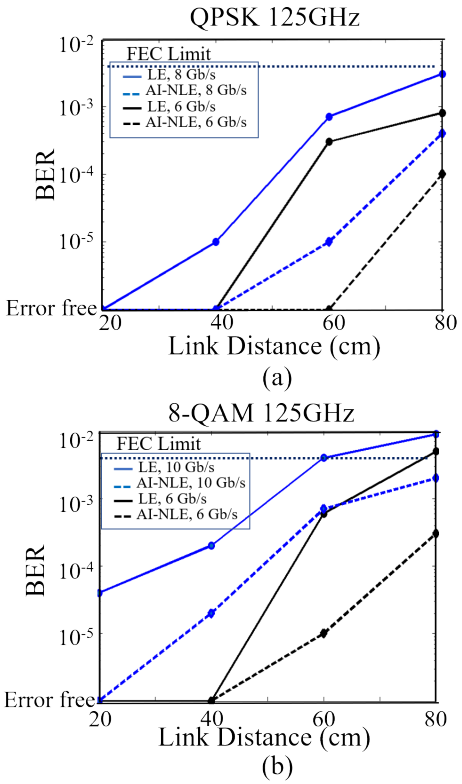

FIGURE 7. Counted BER versus link distance when the carrier frequency is set to 125 GHz for QPSK and 8-QAM OFDM transmissions with NLE-AI equalizer.

cost-effective, with simple and easy-to-maintain structure. by choosing other components (e.g: THz emitter, MZM modulator and high bandwidth detector), employing a coherent detection scheme, high gain antenna, and high gain THz amplifiers, higher data rates and longer wireless link distances are achievable. Future studies focusing on system complexity, system integration, system robustness to environmental changes, and the size/cost of the system are suggested.

V. CONCLUSION

We successfully demonstrated a prototype of a heterogeneous communication system by delivering multiple signal carriers in the same long fiber and segregated datalinks. In the proposed setup, the 3.5 GHz (mid-band) and 28.5 GHz (millimeter -wave band) carrier frequencies, representing 5G links, successfully delivered 1 GHz 16-QAM OFDM signals to the user ends. In sub-THz wireless link, FEC-limit data rates of 4 to 10 Gb/s QPSK and 8-QAM OFDM transmission, over several carrier frequencies from 125 to 225 GHz, covering 100 GHz spectral range, have been achieved at the link distances of <80 cm. The proposed 5G/sub-THz combines multiplexing technique, direct detection, and digital signal processing routine. The system is highly compatible with radio-over-fiber technology, which is cost-effective and easy to deploy. Finally, we utilized an advanced AI-NLE to compensate for the nonlinear effects of transmission channels and components on signal quality. The result indicates the designed AI-NLE compared to linear equalizer significantly improves BER performance of QPSK and 8-QAM signals over 125 GHz carrier frequency. Future researches should focus on reducing costs as much as possible, making the system portable, compact and robust to environmental changes. It is advantageous to design a $1\times N$ array insensitive to polarization emitter combined with a silicon-photonic-based phase array on the transmiter side. This type of arrayed emitter can be used for target tracking. At the same time, it is robust to changes in optical pump polarization, and it is suitable for compact portable THz transmitter. Another potential pathway for a detection scheme is to add another laser tone to shine on the same photomixer and generate a local oscillator simultaneously with the carrier signal to do heterodyne detection to boost SNR while eliminating expensive components. The third suggestion is fabricating c-band lasers in conjunction with a THz photomixer on the same substrate to improve system compactness and reduce the effect of environmental noises on signal.

REFERENCES

[1] S. Ghafoor, N. Boujnah, M. H. Rehmani, and A. Davy, "MAC protocols for terahertz communication: A comprehensive survey," *IEEE Commun. Surveys Tuts.*, vol. 22, no. 4, pp. 2236–2282, 4th Quart., 2020, doi: 10.1109/COMST.2020.3017393.

[2] M. H. Rahaman, A. Bandyopadhyay, S. Pal, and K. P. Ray, "Reviewing the scope of THz communication and a technology roadmap for implementation," *IETE Tech. Rev., Inst. Electron. Telecommun. Eng., India*, vol. 38, no. 5, pp. 465–478, Sep. 2021, doi: 10.1080/02564602.2020.1771221.

[3] C. Chaccour, M. N. Soorki, W. Saad, M. Bennis, P. Popovski, and M. Debbah, "Seven defining features of terahertz (THz) wireless systems: A fellowship of communication and sensing," 2021, *arXiv:2102.07668*.

[4] X. Liu, Q. Sun, W. Lu, C. Wu, and H. Ding, "Big-data-based intelligent spectrum sensing for heterogeneous spectrum communications in 5G," *IEEE Wireless Commun.*, vol. 27, no. 5, pp. 67–73, Oct. 2020, doi: 10.1109/MWC.001.1900493.

[5] K. Shafique, B. A. Khawaja, F. Sabir, S. Qazi, and M. Mustaqim, "Internet of Things (IoT) for next-generation smart systems: A review of current challenges, future trends and prospects for emerging 5G-IoT scenarios," *IEEE Access*, vol. 8, pp. 23022–23040, 2020, doi: 10.1109/ACCESS.2020.2970118.

[6] H. Elayan, O. Amin, B. Shihada, R. M. Shubair, and M.-S. Alouini, "Terahertz band: The last piece of RF spectrum puzzle for communication systems," *IEEE Open J. Commun. Soc.*, vol. 1, pp. 1–32, 2019, doi: 10.1109/OJCOMS.2019.2953633.

[7] M. H. Alsharif, M. A. M. Albreem, A. A. A. Solyman, and S. Kim, "Toward 6G communication networks: Terahertz frequency challenges and open research issues," *Comput., Mater. Continua*, vol. 66, no. 3, pp. 2831–2842, 2021, doi: 10.32604/cmc.2021.013176.

[8] S. Abadal, C. Han, and J. M. Jornet, "Wave propagation and channel modeling in chip-scale wireless communications: A survey from millimeter-wave to terahertz and optics," *IEEE Access*, vol. 8, pp. 278–293, 2020, doi: 10.1109/ACCESS.2019.2961849.

[9] L. U. Khan, "Visible light communication: Applications, architecture, standardization and research challenges," *Digit. Commun. Netw.*, vol. 3, no. 2, pp. 78–88, May 2016, doi: 10.1016/j.dcan.2016.07.004.

[10] I. F. Akyildiz, J. M. Jornet, and C. Han, "Terahertz band: Next frontier for wireless communications," *Phys. Commun.*, vol. 12, no. 7, pp. 16–32, Jan. 2014, doi: 10.1016/j.phycom.2014.01.006.

[11] J. Yu, J. Chen, Z. Li, D. Hou, Z. Chen, and W. Hong, "A 212–260 GHz broadband frequency multiplier chain (×4) in 130-nm BiCMOS technology," in *IEEE MTT-S Int. Microw. Symp. Dig.*, Jun. 2021, pp. 454–457, doi: 10.1109/IMS19712.2021.9575010.

[12] S. Suzuki and M. Asada, "Terahertz oscillators and receivers using electron devices for high-capacity wireless communication," *Proc. SPIE*, vol. 9483, May 2015, Art. no. 948309, doi: 10.1117/12.2183066.

[13] K. Nallappan, H. Guerboukha, C. Nerguizian, and M. Skorobogatiy, "Live streaming of uncompressed HD and 4K videos using terahertz wireless links," *IEEE Access*, vol. 6, pp. 58030–58042, 2018, doi: 10.1109/ACCESS.2018.2873986.

[14] R. Safian, G. Ghazi, and N. Mohammadian, "Review of photomixing continuous-wave terahertz systems and current application trends in terahertz domain," *Opt. Eng.*, vol. 58, no. 11, p. 1, Nov. 2019, doi: 10.1117/1.oe.58.11.110901.

[15] K. Liu, S. Jia, S. Wang, X. Pang, W. Li, S. Zheng, H. Chi, X. Jin, X. Zhang, and X. Yu, "100 Gbit/s THz photonic wireless transmission in the 350-GHz band with extended reach," *IEEE Photon. Technol. Lett.*, vol. 30, no. 11, pp. 1064–1067, Jun. 1, 2018, doi: 10.1109/LPT.2018.2830342.

[16] T. Harter, C. Füllner, J. N. Kemal, S. Ummethala, J. L. Steinmann, M. Brosi, J. L. Hesler, E. Bründermann, A.-S. Müller, W. Freude, S. Randel, and C. Koos, "Generalized Kramers–Kronig receiver for coherent terahertz communications," *Nature Photon.*, vol. 14, no. 10, pp. 601–606, Oct. 2020, doi: 10.1038/s41566-020-0675-0.

[17] T. Nagatsuma, F. Ayano, K. Toichi, L. Yi, M. Fujiwara, N. Iiyama, J. Kani, and H. Ito, "Wireless communication using Fermi-level-managed barrier diode receiver with J-band waveguide-input port," in *IEEE MTT-S Int. Microw. Symp. Dig.*, Aug. 2020, pp. 631–634, doi:10.1109/IMS30576.2020.9224006.

[18] A. Morales, G. Nazarikov, S. Rommel, C. Okonkwo, and I. T. Monroy, "Highly tunable heterodyne sub-THz wireless link entirely based on optoelectronics," *IEEE Trans. THz Sci. Technol.*, vol. 11, no. 3, pp. 261–268, May 2021, doi: 10.1109/TTHZ.2021.3064188.

[19] S. Diebold, K. Nishio, Y. Nishida, J-Y. Kim, K. Tsuruda, T. Mukai, M. Fujita, and T. Nagatsuma, "High-speed error-free wireless data transmission using a terahertz resonant tunnelling diode transmitter and receiver," *Electron. Lett.*, vol. 52, no. 24, pp. 1999–2001, Nov. 2016, doi: 10.1049/EL.2016.2941.

[20] J. Webber, A. Oshiro, S. Iwamatsu, Y. Nishida, M. Fujita, and T. Nagatsuma, "48-Gbit/s 8K video-transmission using resonant tunnelling diodes in 300-GHz band," *Electron. Lett.*, vol. 57, no. 17, pp. 668–669, 2021, doi: 10.1049/ell2.12219.

[21] T. Nagatsuma, M. Sonoda, T. Higashimoto, R. Kimura, L. Yi, and H. Ito, "300-GHz-band wireless communication using Fermi-level managed barrier diode receiver," in *IEEE MTT-S Int. Microw. Symp. Dig.*, Jun. 2019, pp. 762–765, doi: 10.1109/MWSYM.2019.8700954.

[22] W. Zhou, J. Shi, L. Zhao, K. Wang, C. Wang, Y. Wang, M. Kong, F. Wang, L. Cuiwei, J. Ding, and J. Yu, "Comparison of real- and complex-valued NN equalizers for photonics-aided 90-Gbps D-band PAM-4 coherent detection," *J. Lightw. Technol.*, vol. 39, no. 21, pp. 6858–6868, Nov. 1, 2021, doi: 10.1109/JLT.2021.3109126.

[23] C. Wang, K. Wang, Y. Tan, F. Wang, B. Sang, W. Li, W. Zhou, and J. Yu, "High-speed terahertz band radio-over-fiber system using hybrid time-frequency domain equalization," *IEEE Photon. Technol. Lett.*, vol. 34, no. 11, pp. 559–562, Jun. 1, 2022, doi: 10.1109/LPT.2022.3171776.

[24] G. Ancans, V. Bobrovs, A. Ancans, and D. Kalibatiene, "Spectrum considerations for 5G mobile communication systems," *Proc. Comput. Sci.*, vol. 104, pp. 509–516, Jan. 2017, doi: 10.1016/j.procs.2017.01.166.

[25] F.-S. Hsiao, P.-C. Wang, W.-Y. Lin, J.-H. Yan, P. Torkaman, K.-M. Feng, and S.-H. Yang, "A 5G/terahertz integrated wireless network based on wavelength-division multiplexing and terahertz photomixing," in *Proc. 46th Int. Conf. Infr., Millim. THz Waves (IRMMW-THz)*, Aug. 2021, pp. 1–2, doi: 10.1109/IRMMW-THz50926.2021.9567117.

[26] X. Li, L. Deng, X. Chen, M. Cheng, S. Fu, M. Tang, and D. Liu, "Modulation-format-free and automatic bias control for optical IQ modulators based on dither-correlation detection," *Opt. Exp.*, vol. 25, no. 8, p. 9333, Apr. 2017, doi: 10.1364/oe.25.009333.

[27] S. Nellen, T. Ishibashi, A. Deninger, R. B. Kohlhaas, L. Liebermeister, M. Schell, and B. Globisch, "Experimental comparison of UTC- and PIN-photodiodes for continuous-wave terahertz generation," *J. Infr., Millim., THz Waves*, vol. 41, no. 4, pp. 343–354, Apr. 2020, doi: 10.1007/s10762-019-00638-5.

[28] S. Zhou, Y. Song, Y. Tan, L. Zhang, Y. Li, J. Ye, and R. Lin, "Performance of optical OFDM transmission over RoF system with Mach–Zehnder modulator," in *Proc. Asia Commun. Photon. Conf. Exhib. (ACP)*, Nov. 2011, pp. 1–6, doi: 10.1117/12.903898.

[29] H. K. Shankarananda, "External modulators and mathematical modeling of Mach–Zehnder modulator," *Int. J. Innov. Sci. Eng. Technol.*, vol. 3, no. 12, pp. 214–220, 2016. [Online]. Available: https://www.ijiset.com/

[30] L. Zhang, M. Qiao, S. Wang, Z. Lu, L. Zhang, X. Pang, X. Zhang, and X. Yu, "Nonlinearity-aware optoelectronic terahertz discrete multitone signal transmission with a zero-bias diode," *Opt. Lett.*, vol. 45, no. 18, p. 5045, Sep. 2020, doi: 10.1364/OL.401414.

[31] G. S. Yadav, C.-Y. Chuang, K.-M. Feng, J.-H. Yan, J. Chen, and Y.-K. Chen, "Reducing computation complexity by using elastic net regularization based pruned Volterra equalization in a 80 Gbps PAM-4 signal for inter-data center interconnects," *Opt. Exp.*, vol. 28, no. 26, p. 38539, Dec. 2020, doi: 10.1364/OE.411465.

[32] G. S. Yadav, C.-Y. Chuang, K.-M. Feng, J. Chen, and Y.-K. Chen, "Computation efficient sparse DNN nonlinear equalization for IM/DD 112 Gbps PAM4 inter-data center optical interconnects," *Opt. Lett.*, vol. 46, no. 9, p. 1999, May 2021, doi: 10.1364/OL.417834.

[33] M. Hudlicka, C. Lundstrom, D. A. Humphreys, and I. Fatadin, "BER estimation from EVM for QPSK and 16-QAM coherent optical systems," in *Proc. IEEE 6th Int. Conf. Photon. (ICP)*, Mar. 2016, pp. 1–3, doi: 10.1109/ICP.2016.7510025.

[34] C. Castro, S. Nellen, R. Elschner, I. Sackey, R. Emmerich, T. Merkle, B. Globisch, D. de Felipe, and C. Schubert, "32 GBd 16 QAM wireless transmission in the 300 GHz band using a PIN diode for THz upconversion," in *Proc. Opt. Fiber Commun. Conf. (OFC)*, 2019, pp. 4–6.

[35] H. T. Friis, "A note on a simple transmission formula," *Proc. IRE*, vol. 34, no. 5, pp. 254–256, May 1946, doi: 10.1109/JRPROC.1946.234568.

[36] T. A. Eriksson, H. Bülow, and A. Leven, "Applying neural networks in optical communication systems: Possible pitfalls," *IEEE Photon. Technol. Lett.*, vol. 29, no. 23, pp. 2091–2094, Dec. 1, 2017, doi: 10.1109/LPT.2017.2755663.

[37] Z. Wan, J. Li, L. Shu, M. Luo, X. Li, S. Fu, and K. Xu, "Nonlinear equalization based on pruned artificial neural networks for 112-Gb/s SSB-PAM4 transmission over 80-km SSMF," *Opt. Exp.*, vol. 26, no. 8, p. 10631, Apr. 2018, doi: 10.1364/oe.26.010631.

[38] S. Yadav, T. Tsuritani, S. Beppu, H. Takahashi, I. Morita, K.-M. Feng, and J.-H. Yan, "Dynamic complex deep neural network nonlinear equalizer for 64 QAM long-haul transmission systems," in *Proc. 24th Optoelectron. Commun. Conf. (OECC) Int. Conf. Photon. Switching Comput. (PSC)*, Jul. 2019, pp. 1–3.

[39] S. Liu, M. Xu, J. Wang, F. Lu, W. Zhang, H. Tian, and G.-K. Chang, "A multilevel artificial neural network nonlinear equalizer for millimeter-wave mobile fronthaul systems," *J. Lightw. Technol.*, vol. 35, no. 20, pp. 4406–4417, Oct. 15, 2017, doi: 10.1109/JLT.2017.2717778.

[40] G. S. Yadav, C.-Y. Chuang, K.-M. Feng, J. Chen, and Y.-K. Chen, "Computation efficient sparse DNN nonlinear equalization for IM/DD 112 Gbps PAM4 inter-data center optical interconnects," *Opt. Lett.*, vol. 46, no. 9, p. 1999, May 2021, doi:10.1364/OL.417834.

POUYA TORKAMAN was born in Hamedan, Iran, in 1992. He received the M.A. degree in electrical engineering from Tarbiat Modares University, Tehran, Iran, in 2017. Currently, he is pursuing the Ph.D. degree with the Institute of Electronics, National Tsing Hua University, Taiwan. His research interests include design and fabrication of new generations of THz radiation sources for THz communication systems, THz communication systems, and fiber communication.

GOVIND SHARAN YADAV was born in Amethi, Uttar Pradesh, India, in 1985. He received the Ph.D. degree from the Institute of Photonics Technologies, National Tsing Hua University, Hsinchu, Taiwan. In 2018, he did the Internship Program at the Photonic Transport Network Laboratory, KDDI Research, Japan. He is currently employed as a full-time research and development employee at IC Plus Corporation, as well as a Researcher with Prof. Feng's laboratory at the National Tsing Hua University. His research interests include machine learning, deep learning, compressive sensing and sparse signal processing for high-capacity long-haul wavelength-division-multiplexed (WDM) transmission systems, data-center optical interconnects, and THz communication systems.

PO-CHUAN WANG received the B.Sc. degree in electronic engineering from the National Kaohsiung University of Science and Technology, Kaohsiung, Taiwan, in 2016, and the M.Sc. degree from the Institute of Photonic Technology, National Tsing Hua University, Hsinchu, Taiwan, in 2021, specializing in radio over fiber. His research interests include fiber/wireless communication and digital signal processing.

TUNG-YU LU is currently an undergraduate student of Interdisciplinary Program of Engineering with the National Tsing Hua University, Hsinchu, Taiwan. His research interest includes design and simulation of 6G terahertz communication systems.

XUAN-WEI MIAO is currently pursuing the degrees in electronic engineering (EE) and economics (ECON) with the National Tsing Hua University. He is focusing on communication, where his research interest includes the design and simulation of terahertz wireless communication systems.

FANG-SUNG HSIAO received the B.S. degree in electrical engineering and the M.S. degree in electronic engineering from the National Tsing Hua University, Taiwan, in 2018 and 2020, respectively.

Since 2021, he has been a RF Product Engineer with Qualcomm. He has established contributions to the development of terahertz systems, wireless communication, and fiber communication.

Dr. Hsiao received several prestigious awards and scholarships including, Government Pilot Overseas Scholarship, in 2018 and 2020; IEEE young Professional Artic Challenge First Prize, in 2018; Government International Visiting Scholarship, in 2019; and ATIDA THz Innovation and Technique Application First Prize, in 2020.

KAI-MING FENG (Member, IEEE) received the B.S. degree from the National Taiwan University, Taipei, Taiwan, in 1992, and the M.S. and Ph.D. degrees from the University of Southern California, Los Angeles, in 1995 and 1999, respectively, all in electrical engineering. In 1999, he was with Chunghwa Telecommunications Laboratories, Taoyuan, Taiwan, as a Research Fellow. In 2000, he joined Phaethon Communications Inc., Fremont, CA, USA, to conduct the company's main products at 40-Gb/s wavelength division multiplexing (WDM) systems. He then joined the Institute of Communications Engineering, the Institute of Photonics Technologies, and the Department of Electrical Engineering, National Tsing Hua University, Hsinchu, Taiwan, as an Assistant Professor. He is currently a Full Professor at these institutes. His current research interests include digital signal process technologies for high speed PAM4 signals, integrated radio-over-fiber techniques for wireless downlinks and uplinks in 5G mobile front haul systems, and millimeter wave and terahertz communication systems.

SHANG-HUA YANG (Member, IEEE) received the B.S. degree in electrical engineering from the National Tsing Hua University (NTHU), Taiwan, in 2007, the M.S. degree in electro-optical engineering from the National Chiao Tung University, Taiwan, in 2009, and the Ph.D. degree in electrical engineering from the University of Michigan, Ann Arbor, in 2016.

Since 2017, he has been a Tenure-Track Assistant Professor with the Department of Electrical Engineering, NTHU. He has established contributions to the development of ultrafast electronics, microwave photonics, terahertz optoelectronics, integrated terahertz systems, as well as plasmonic photonics applications. The outcomes of his research have appeared in over 80 refereed papers in peer-reviewed journals and conference proceedings on these topics.

Dr. Yang received several prestigious awards and scholarships including, SPIE Scholarship in Optics and photonics, in 2012; IEEE Antennas and Propagation Society Doctoral Research Award, in 2014; Joan and Irvin Jacobs TIX Institute Industry Scholar, in 2017 and 2018; MOST Young Scholar Fellowship, in 2018; and Human Frontier Science Program Research Grant Award, in 2020. He has been the Co-Founder and the Deputy Director of NTHU Terahertz Optics and Photonics Center, since 2019.